Title

In search of long-term hemispheric asymmetry in the geomagnetic field: Results from high northern latitudes

Journal

Geochemistry, Geophysics, Geosystems, 14(8)

ISSN

15252027

Authors

Cromwell, G.
Tauxe, L.
Staudigel, H.
et al.

Publication Date

2013-08-01

DOI

10.1002/ggge.20174

In search of long term hemispheric asymmetry in the geomagnetic field: results from high northern latitudes

G. Cromwell,[1] L. Tauxe,[1] H. Staudigel,[2] C.G. Constable,[2], A.A.P. Koppers,[3] R-B. Pedersen[4]

Abstract. Investigations of the behavior of the geomagnetic field on geological time-scales rely on globally distributed datasets from dated lava flows. We present the first suitable data from the Arctic region, comprising 37 paleomagnetic directions from Jan Mayen (71°N, 0.2-461 ka) and Spitsbergen (79°N, 1-9.2 Ma) and 5 paleointensity results. Dispersion of the Arctic virtual geomagnetic poles over the last 2 Ma ($27.3\pm4.0°$) is significantly lower than that from published Antarctic datasets ($32.1 \pm 5.0°$). Arctic average virtual axial dipole moment (76.8 ± 24.3 ZAm^2) is high in comparison with the same time interval (34.8 ± 8.2 ZAm^2), although the data are still too sparse in the Arctic to be definitive. These data support a long-lived hemispheric asymmetry of the magnetic field, contrasting higher, more stable fields in the north with lower average strength and more variable field directions in the south. Such features require significant non-axial-dipole contributions over 10^5-10^6 years.

1. Introduction

The fundamental assumption used for plate reconstructions is that when averaged over geological timescales, the Earth's magnetic field can be approximated by a geocentric axial dipole (GAD). This simplicity is reflected in many geomagnetic field models derived from observations and numerical geodynamo simulations of convection in the Earth's liquid outer core. However, significant departures from a GAD field are observed in the present field (SA in Figure 1), and measurements over historical and archaeological time scales (e.g., *Korte et al.* [2011]) indicate that non-axial-dipole effects persist at least over the last 10 kyr. In this paper we explore the geomagnetic field over geological time scales at high latitude and demonstrate long lived asymmetries in field behavior between the northern and southern hemispheres. This asymmetry has consequences for models explaining the origin of the Earth's magnetic field, particularly those that invoke variations in heat flux at the core-mantle boundary to explain changes in reversal rate, long term departures from GAD in the time-averaged field, and geographical variations in paleosecular variation (e.g., *Glatzmaier et al.* [1999]; *Bloxham* [2000]).

The GAD hypothesis predicts that geomagnetic intensity should be twice as strong at the poles as at the equator and that inclination will vary with latitude according to the following equation:

$$tanI = 2tan\lambda \tag{1}$$

where I is inclination and λ is latitude. Early compilations of paleointensity data (e.g., *Tanaka et al.* [1995]) and directional data (e.g., *Opdyke and Henry* [1969]) appeared to support the GAD hypothesis with only minor deviations (e.g., *Wilson* [1971]). Moreover, models of secular variation of an essentially GAD field (e.g., *Constable and Parker* [1988]; *McElhinny and McFadden* [1997]; *Tauxe and Kent* [2004]; *Linder and Gilder* [2012]) produce directional scatter that is symmetric about the equator.

The modern geomagnetic field (Figure 1) exhibits significant hemispheric asymmetries that deviate significantly from an axial-dipole field. Northern hemisphere field structure is controlled by two high-intensity flux lobes at high latitudes, while the southern hemisphere is dominated by the low-intensity South Atlantic anomaly and a single high-latitude flux lobe. The South Atlantic anomaly is a regional, non-zonal structure that historically is associated with low average field strengths and high scatter [*Korte and Constable*, 2005]. If such features are persistent over million year timescales we would expect to see northern high latitude fields with low directional scatter and high paleointensities, while observing southern hemisphere paleofields similar to those observed in Antarctica [*Lawrence et al.*, 2009].

Lawrence et al. [2009] collected paleointensity (47) and directional (125) estimates from Antarctica spanning the last 13 Ma. Surprisingly, their paleointensity data showed no high latitude enhancement of field strength, and the directional data were significantly more scattered than predicted by standard paleosecular variation models (e.g., *Constable and Parker* [1988]; *McElhinny and McFadden* [1997]; *Constable and Johnson* [1999]; *Tauxe and Kent* [2004]). To date there are no suitable Arctic ($> 66°$N) data sets with which to compare to Antarctica and establish whether the observed Antarctic field behavior is symmetrical at high latitudes, or if it is unique to the southern hemisphere. We present here paleomagnetic data from expeditions to the Arctic islands of Jan Mayen and Spitsbergen that are consistent with the prediction of asymmetrical field behavior at high latitudes.

2. Geology and Sampling

2.1. Jan Mayen

Jan Mayen is a volcanic island dominated by the Earth's northernmost active volcano, Beerenberg (2277 m above sea level). Jan Mayen (Figure 2a) sits in the North Atlantic Ocean, just south of the Jan Mayen Fracture Zone between the Mohns and Kolbeinsey Ridges. *Imsland* [1978] estimated surface volcanism to be approximately 400 ka or younger based on a set of ^{40}K/^{40}Ar dates by *Fitch et al.* [1965] and *Duncan, R., unpublished*. *Fitch et al.* [1963] collected paleomagnetic samples from ten cooling units on the flanks of Beerenberg. These were of uniformly normal polarity. The oldest surface flows on Jan Mayen are part of the Havhestberget formation, a group of submarine hyaloclastites which can be found in the

[1]Geosciences Research Division, Scripps Institution of Oceanography, University of California San Diego, La Jolla, California, USA

[2]Institute of Geophysics and Planetary Physics, Scripps Institution of Oceanography, University of California San Diego, La Jolla, California, USA

[3]College of Earth, Ocean and Atmospheric Sciences, Oregon State University, Corvallis, Oregon, USA

[4]Department of Earth Science, Centre for Geobiology, University of Bergen, Bergen, Norway

southwestern (Sör-Jan) and mid-sections (Midt-Jan) of the island. Overlying the Havhestberget formation are the subaerially erupted Nordvestkapp formation and the more recent Inndalen formation. These constitute the majority of surface volcanics and are found throughout the island. Historical lava flows date back to 1732 [*Imsland*, 1978] and are found in the northwest of the island (Nord-Jan), proximal to Beerenberg. The geology, geochemistry and petrology of the island is described extensively by *Imsland* [1978] and *Imsland* [1980].

We collected oriented samples from 23 sites in August 2009. Our sampling strategy was to target each of the geologic formations described above (Havhestberget, Nordvestkapp and Inndalen) and our individual site selection was guided by several unpublished ^{40}K/^{40}Ar dates [*Duncan, R., unpublished*] and by outcrop accessibility. Two Havhestberget exposures were sampled, one in the southern sea cliffs of Sör-Jan (JM012) and the other in sea cliffs along the north coast of Midt-Jan (JM006-009). Sör-Jan is dominated by a low-lying plateau of Inndalen lavas to the north (JM003, JM013-015), while the southern highland regions contain a mixture of Inndalen scoria and trachyte cones and older Nordvestkapp lavas (JM002, JM004, JM011, JM021-023). Midt-Jan consists predominantly of Nordvestkapp lavas and unconsolidated beach and lagoonal sediment. Nord-Jan lava flows radiate out from Beerenberg and consist of interfingered Inndalen (JM024, JM019-020, JM025-027) and Nordvestkapp lavas (JM016-017). Sampling beyond the southwestern slope of Beerenberg was inhibited by steep cliffs along the shoreline and glacial ice.

All samples taken in Jan Mayen were oriented with magnetic compass and either sun compass or a ProMark3 differential GPS system (Figure A1). Certain samples were oriented with all three methods. Care was taken avoid oversampling the same geomagnetic field state by only sampling nearby/overlying lava flows if geologic evidence for temporal gaps could be determined.

2.2. Spitsbergen

Spitsbergen is an island in the northwest of the Svalbard archipelago, on the northwestern edge of the Barents shelf in the North Atlantic (Figure 2b). The geology of Svalbard is dominated by fold-thrust belts associated with Paleozoic tectonics [*Lyberis and Manby*, 1999; *Dewey and Strachan*, 2003; *Torsvik et al.*, 2001] and the Cenozoic opening of the Norwegian-Greenland Sea [*Talwani and Eldholm*, 1977; *Maher et al.*, 1995]; for a detailed description of the the geology of the island see, e.g., *Harland* [1997].

There are two phases of Neogene volcanic activity in the Woodfjord region [*Vagnes and Amundsen*, 1993] where our sampling is concentrated. A thick sequence of tholeiitic plateau basalts have an age of 9-12 Ma [*Prestvik*, 1977] lie to the east of Woodfjord. A second pulse of volcanism to the west of Woodfjord is exposed in three eruptive centers [*Skjelkvale et al.*, 1988]: Sverrefjell, Halvdanpiggen and Sigurdfjell. Preliminary paleomagnetic data [*Halvorsen*, 1972] suggest that Sverrefjell is normally magnetized, consistent with K-Ar dates giving an upper age limit of $<$1 Ma [*Burov and Zagruzina*, 1976]. *Halvorsen* [1972] also reported reversely magnetized lavas from nearby Halvdanpiggen, but the directions were anomalously shallow and could be Brunhes age excursions. The three centers are of nearly identical geochemistry and are arrayed along the same N-S fault line. Sverrefjell erupted during and prior to the last major glaciation in Bockfjord, believed to have occurred between about 100 and 250 ka [*Skjelkvale et al.*, 1988]. Geomorphological and geochemical arguments suggest that Sigurdfjell is approximately the same age as Sverrefjell while Halvdanpiggen may be somewhat older.

In July 2001 we collected oriented samples from 14 independent lava flows. Two sites are from Sverrefjell (SP100-101), two from Halvdanpiggen (SP102-103) and one site from Sigurdfjell (SP104) (all sites $<$1 Ma). The remaining sites (SP105-113) derive from the earlier eruptive phase (9-12 Ma) to the east of Woodfjord (see Figure 2b). Various lithologies were sampled including pahoehoe lava flows, palagonite tuffs and basaltic dikes. Care was taken to collect samples where there was no evidence of tilting, slumping or any frost heaving effects.Samples taken in Spitsbergen were oriented by magnetic compass and either sun compass or a Beeline differential GPS system (Figure A2, described by *Lawrence et al.* [2009] and *Tauxe* [2010]).

3. Reliability of Orientation Methods at High Latitude

Two thirds (22/36) of our northern high latitude sample sites in this study were oriented, at least in part, by differential GPS systems, either the Beeline baseline system or the ProMark3 described in the previous sections. The recent Antarctic study by *Lawrence et al.* [2009] also used the Beeline system to orient 28 out of 129 sites. These three study areas (Jan Mayen, Spitsbergen and Antarctica) represent the bulk of published high latitude paleomagnetic data and all known sites oriented by differential GPS systems, therefore an evaluation of the reliability of the differential GPS orientation method is in order.

We use sun compass azimuths as the standard for evaluating the differential GPS method because of its widespread use in the paleomagnetic community as a reliable orientation method. Uncertainties in sun compass orientations are estimated to be about 3° [*Tauxe*, 2010] and derive from errors in the field orientation process (e.g. improper insertion of the Pomeroy into the drill hole, deviations of the Pomeroy from horizontal, the width of the gnomon, and uncertainties in time and location of the measurement).

A total of 241 samples and 37 sites were oriented with magnetic compass in addition to either sun or differential GPS (or both). Magnetic azimuths were corrected to "true north" using the IGRF predicted declinations for each location. Because all samples were oriented with either sun compass or differential GPS methods, we did not routinely check the magnetic azimuths by backsighting, however there are a total of 63 samples whose orientations were estimated with backsighted azimuths of which 23 were also oriented with a sun compass.

Azimuths obtained from the differential GPS systems were evaluated by 1) comparing GPS and sun compass directions on samples where both were measured (total of 198 samples, Figure 3a) and 2) by comparing the site level directional scatter obtained from the two methods on sites where both were measured (total of 24 sites, Figure 3b). The first approach gives us a measure of the agreement between the two methods at the sample level and the second tells us which method is the most effective at reducing site level scatter, hence, which is the most precise.

In Figure 3a we compare the deviations of Beeline (dark blue) and ProMark3 (red) GPS samples, magnetic compass (purple) and backsighted (light blue) azimuths to sun compass azimuths. These are plotted as cumulative distribution functions (CDFs).

Magnetic compasses are very precise instruments, however the range of azimuth deviations in Figure 3a confirm the widely held belief that their orientations cannot be trusted when used on lava flows, at least at high latitudes. 48% of magnetic compass azimuths fall within 5° of sun compass estimates. Backsighting in the field is generally thought to minimize, and even remove, the effects of magnetization from lava flows, however, our backsighted azimuths are very asymmetric about 0° and only 17% are within 5° of sun compass azimuths. Backsight and magnetic compass MAD* values are equivalent, indicating that backsighting does not improve overall orientation accuracy and should not be relied upon to correct magnetic deviations in the field.

Both differential GPS methods perform significantly better than magnetic compasses (MAD* values of 1.6° and 6.3°, respectively) even with the presence of a few large outliers. 95% of all GPS orientations deviate less than 13.9° from their respective sun compass azimuths and approximately 73% of GPS azimuths deviate less than 5°. Two deviant samples oriented with the ProMark3 (samples JM021i and JM021j, marked with white "+"s in Figure 3a) are determined to be caused by insufficient satellite coverage and are not included in GPS statistics. Four samples from the Beeline system have deviations greater than 30°, and although the source of

uncertainty cannot be determined it is certain that these are erroneous measurements. GPS statistics change considerably if these four samples are excluded (All GPS: σ = 5.21°, MAD* = 1.59°; Beeline GPS: σ = 4.8°, MAD* = 1.16°).

Significant GPS orientation errors are rare (6/296 samples) but if undetected could affect site mean directions. By implementing appropriate minimum criteria for site level precision, such as α_{95} or the Fisher precision statistic k, sites with inaccurately oriented samples will be removed from PSV analysis.

Figure 3b shows the scatter in directions observed at the site level as a second measure of precision in orientation. We compare the circular standard deviation (CSD) of site level mean directions on 14 sites oriented with sun compass, differential GPS, and magnetic compass. For comparison we also plot equivalent values of the estimated precision statistic, k. Interestingly, magnetic compass orientations perform as well or better than both sun compass and GPS in terms of CSD. This observation can be attributed to the high precision of magnetic compasses. GPS orientations with poor precision (relative to sun compass measurements) should result in site means with large angular deviations and sites oriented with GPS do appear on average to be slightly less precise than when oriented with a sun compass. However the k for all GPS oriented sites is still greater than 50, a selection criterion on a recent study of PSV in lava flows [*Johnson et al.*, 2008], and all but one site have ks greater than 183 or a CSD of less than 6°.. As there does not appear to be a systematic bias in directions, the uncertainty in GPS orientation at high latitude does not appear to be a serious problem. GPS orientation systems are therefore suitable alternatives to the sun compass, especially at high latitudes where sunshine may be scarce and the accuracy exceeds magnetic compass measurements alone.

4. ^{40}Ar/^{39}Ar Geochronology

^{40}Ar/^{39}Ar incremental heating experiments were successful on ten sites from Jan Mayen and three from Spitsbergen (Figure A3, Table A1). Ages from Jan Mayen ranged from 6 ka to 460.9 ka. We attempted to date sites believed to be old enough for successful ^{40}Ar/^{39}Ar dating experiments, however one site, JM022, returned an exceptionally low age that should be considered with some caution, 6.0 ± 14.5 ka. Site JM020 is thought to be the 1732 CE historical eruption *Imsland* [1978] and site JM019 is a surface flow in proximity to JM020. With no other age information we designate JM019 as "historical" (<2000 years). All other Jan Mayen sites not dated are believed to be too young for ^{40}Ar/^{39}Ar dating.

Sites SP100-104 were taken from a younger volcanic episode of 100-250 ka. Successful ages from Spitsbergen reported here ranged from 8.32 to 9.15 Ma, consistent with the age estimates for earlier Neogene volcanic episodes. Sites SP106-108, SP110, SP112, and SP113 are part of the same volcanic province as SP109 and SP111 and are therefore assigned equivalent ages of 9 Ma.

5. Paleointensity

We used the IZZI modified Thellier-Thellier paleointensity experiment [*Tauxe and Staudigel*, 2004] to estimate intensity for Spitsbergen and Jan Mayen specimens (see Auxiliary Material). Figure 5 shows examples of representative IZZI experiments as Arai plots [*Nagata et al.*, 1963]. Insets are the behavior of the remanence (zero-field steps) plotted as Zijderveld diagrams [*Zijderveld*, 1967].

There is general consensus in the paleointensity community that specimens with straight lines in the Arai plots, with no evidence of alteration (pTRM checks plot on top of initial pTRM measurements) or multi-component behavior in the Zijderveld diagrams, can be used to estimate the ancient magnetic field strength (e.g. Figure 5). However such data are rather rare and there is little agreement on how to properly select or reject data that depart from ideal behavior (e.g. Figure 5b, c and d). Recent paleointensity studies tend to require more stringent specimen level selection criteria with the goal of removing data that significantly depart from ideal behavior (e.g. *Shaar et al.* [2011]).

In our experiments, some specimens acquired a remanence parallel to the laboratory field which was not demagnetized by later heating steps (e.g., Figure 4b). In some cases, this behavior is less pronounced, only manifesting itself after 95% of the NRM has been removed (e.g., Figure 4c). Moreover, many specimens exhibit concave-up curves in the Arai plots, Figure 4d. Such behavior is usually interpreted as characteristic of multi-domain remanences (e.g., *Dunlop and Özdemir* [2001]). To screen out multi-component remanences or experiments that exhibited alteration, we have used the following strategy (see Table A2 and *Tauxe* [2010] for definitions): 1) Each specimen must have a relatively linear component of magnetization representing a majority of the TRM applied to the specimen ($f_{vds} \geq 0.7$) with a maximum angle of deviation (MAD)$\leq$ 5; 2) no data can be used at temperature steps greater than a failed pTRM check as defined by a DRAT of 20%; 3) the temperature range of the interpreted intensity component must be related to the characteristic remanent magnetization of the specimen (DANG $\leq$13); 4) no temperature step may be used where the pTRM gained is lower than the gain of the previous temperature step.

At the site level, we require at least two intensity estimates per site, $N_B \geq 2$, and evaluate the percent standard deviation of the mean intensity, which is $d\sigma_B = 100 \times \sigma_B/B$. We use a $d\sigma_B$ cutoff of 15% in order to ensure that outliers do not adversely effect our final paleointensity estimation.

As illustrated in Figure 4c and d, some specimens display concave-up Arai plots. Selecting the low-temperature component results in a steeper slope and therefore a high ancient field estimate while selecting the high temperature component results in a shallower slope and a smaller ancient field. While either of these selections could meet the criteria outlined above, they are incompatible with each other and it is difficult to justify choosing one over the other. *Dunlop and Özdemir* [2001] suggest that the appropriate measure of paleointensity for multi-domain specimens is normalizing by the full TRM, i.e., by taking the first and last temperature steps of the IZZI experiment. To ensure that the full vector is used in the paleointensity calculation of specimens with sagged Arai plots, we required the value of f_{vds} to be at least 0.95. If the implications of *Dunlop and Özdemir* [2001] are correct, all specimens from a given site should yield the same answer and pass our site selection criterion.

Our attempts to define the intensity component for concave up experiments using the total TRM resulted in highly variable within-site field estimates which exceeded our 15% cutoff for $d\sigma_B$. Interestingly, all the estimates derived from curved Arai plots were lower than those derived from straight Arai plots from the same site. Moreover, when given a fresh laboratory TRM and treated to a second IZZI experiment, all of our specimens behaved in an ideal fashion so the curvature was not reproducible on laboratory time scales.

Shaar et al. [2011] conducted a series of experiments on synthetic multi-domain specimens and observed a decay of NRM intensity in multi-domain specimens, without the acquisition of secondary directional components, over a time span of several years. Specimens showing this behavior would not fail pTRM checks or DANG criteria but will yield paleointensity estimates that are too low. All aberrant experiments observed by *Shaar et al.* [2011] were markedly concave up. The evident variability of total and partial TRM estimates for concave-up specimens has lead us to reject all multi-domain paleointensity estimates until some constraint can be placed on the reliability of concave-up Arai plots.

Despite our reluctance to include specimens displaying concave-up Arai Plots, a few exceptions were made for specimens from three sites where we determined that the observed behavior was not actually multi-domain (Figure 4c). Specimens from sites JM002, JM019 and JM020 are included because the concavity of the Arai plot begins after a failed pTRM check, indicating that alteration is a plausible cause of this behavior. Arai plots in each of these cases

are relatively straight prior to the failed pTRM check and pass all specimen level criteria (1-4). It can be assumed that if alteration did not occur then the slope of the intensity component would have continued through the remainder of the IZZI experiment. We therefore assume that the straight, lower-temperature intensity component, before the failed pTRM check, is an accurate estimate of the ancient magnetic field in each specimen. If our interpretation is incorrect and the observed behavior in these specimens is not caused by alteration, then the low temperature components we selected would likely overestimate the ancient magnetic field strength (e.g., Figure 4d, purple component).

Five sites from Jan Mayen (Table 1, Figure 7) meet our selection criteria while no samples from Spitsbergen are deemed reliable. The majority of those specimens that failed our selection criteria altered during the multiple heatings of the IZZI experiment. The average intensity of our Jan Mayen data set (n=5) is 56.9 ± 18.0 μT (σ) with an equivalent virtual axial dipole moment (VADM) of 76.8 ± 24.3 ZAm^2 (σ). This data set exhibits the high latitude enhancement of field strength expected from a GAD field, and is nearly a factor of two higher than comparably-aged data from Antarctica (n=7), 26.8 ± 6.0 μT (σ) and 35.3 ± 7.9 ZAm^2 (σ) [*Lawrence et al.*, 2009].

6. Paleodirections

We demagnetized at least five specimens per site using alternating field (AF) and thermal demagnetization techniques (see Auxiliary Material). Principal component analysis [*Kirschvink*, 1980] was used to determine characteristic directions or best fit planes for each specimen. Generally, uni-vectorial decay was fit with a line while data affected by laboratory overprints like pTRM acquisition were fit by planes. The assumption here is that the original characteristic direction is constrained to lie within the best-fit plane. Specimen lines and planes were deemed acceptable if they had at least four consecutive demagnetization steps and a maximum angle of deviation (MAD) $\leq 5^\circ$.

Two types (Type I and II) of site level demagnetization behavior were observed. Type I sites (7 total, e.g., Figure 5a-c) decayed linearly to the origin in both AF and thermal demagnetization experiments for all specimens. Type II sites (30 total, e.g., Figure 5d-i) were categorized by some specimens exhibiting laboratory overprints. Site means for Type I sites (Figure 5c) were calculated using Fisher statistics [*Fisher*, 1953] and the combined lines and planes method of *McFadden and McElhinny* [1988] was used for Type II sites (Figure 5f). We required all sites to have a minimum of five specimens (n$\geq$ 5), a Fisher precision parameter, κ, $\geq$ 50 and a demagnetization code (DC) of 4 or 5 [*McElhinny and McFadden*, 2000] (complete demagnetization, use of PCA). See Tables 2 and 3 for all acceptable site mean directions and virtual geographic poles (VGPs).

Several lava flows have overlapping directions (e.g., JM009 and JM013; JM011 and JM020; SP106 and SP107) but there is no indication of preferentially oversampling any temporal field since all the sites in question are from geographically distinct units and/or show evidence of temporal gaps between units (e.g., paleosols).

Figure 6 shows equal area plots of site mean directions (a, b) and orthographic plots of site VGPs (c, d) for the two locations. Combined site mean directions for each of the Jan Mayen and Spitsbergen locations (green triangles) are consistent with those expected from a GAD field (stars). Reverse polarity sites from Spitsbergen are antipodal to normal sites and the data pass both Watson's V_w and a bootstrap reversals tests [*Tauxe*, 2010]. Combining the antipodes of the reverse directions produces distributions with estimated κ_Fs of 36 and 27 for Jan Mayen and Spitsbergen respectively and there are no transitional or excursional directions in our data set.

It has become traditional to use the statistic S of *Cox* [1969] to quantify VGP scatter. We modify S and use the statistic S_F [*McElhinny and McFadden*, 1997] in order to correct for within-site directional scatter.

$$S_F = \sqrt{(N-1)^{-1} \sum_{i=1}^{N} ((\Delta_i)^2 - \frac{{S_w}^2}{nn_i})}, \qquad (2)$$

where N is the number of sites, Δ_i is the angle between the i^{th} VGP and the spin axis, S_w is within-site scatter (defined as $81^\circ/\sqrt{k_w}$, where k_w is the Fisherian precision statistic), and nn_i is the number of specimens in the i^{th} site. We list S_F for the Jan Mayen and Spitsbergen data sets in Table 4.

Jan Mayen and Spitsbergen site VGPs (Figure 6c, d) are highly scattered (κ_Fs of 11 and 10, respectively) as a consequence of the VGP mapping at high latitudes. The dotted black circles represent the 45° colatitudinal VGP cutoff often applied in PSV studies (e.g., *McElhinny and McFadden* [1997]). Four sites have VGP latitudes close to this arbitrary cutoff and two (JM016, SP102) exceed the cutoff. The use of VGP cutoffs (e.g., 45° or that of *Vandamme* [1994]), has been shown to bias paleosecular variation estimates (e.g., *Lawrence et al.* [2006]) by arbitrarily defining some directions as transitional. This same bias is exaggerated at high latitudes.

Jan Mayen has 23 directional sites, all younger than 461 ka, and an unfiltered VGP scatter estimate of $24.4^{29.4^\circ}_{19.1}$. Spitsbergen has 13 directional sites, unevenly distributed at $<$ 1 Ma (n=5) and 9 Ma (n=9), with VGP scatter of $28.0^{35.6^\circ}_{20.3}$. Jan Mayen and Spitsbergen are at different latitudes and have two distinct age distributions, $<$ 1 Ma and $\sim$9 Ma and Spitsbergen has too few data points in either age group to stand alone. However, if we combine the data from Jan Mayen and the younger Spitsbergen group together, the S_F values cannot be distinguished ($27.3^{32.1^\circ}_{21.9}$ (n=28) from the older Spitsbergen group alone $20.6^{26.5^\circ}_{14.2}$ (n=9)). Therefore we combine the two data sets despite their spatial and temporal differences. When combined (JM/SP) these data represent the first estimate for directional and VGP scatter at Arctic latitudes (average of 74.2°N); S_F for these data (Figure 8a) is $25.4^{29.8^\circ}_{21.1}$ (n=37, 0-9 Ma) and is significantly lower than that estimated for the Antarctica data of *Lawrence et al.* [2009] of $32.7^{36.8^\circ}_{28.9}$ (n=131, 0-13 Ma). Note that no VGP filter was used for either calculation.

7. Discussion

New directional and paleointensity results suggest the possibility of hemispheric asymmetry at high latitudes. The five Jan Mayen intensity sites span the last 300 kyr, with an average VADM of 76.8 ± 24.3 ZAm^2, as do seven sites from Antarctica, 35.3 ± 7.9 ZAm^2. Only one Jan Mayen site (JM021) has a comparable age with any Antarctic sites (mc35, mc217), too few for a comprehensive comparison. To augment the Arctic data set we search the MagIC database (http://earthref.org/MAGIC) for published data from from the last 300 kyr at high latitudes ($\geq 60^\circ$) and find three studies [*Pesonen et al.*, 1995; *Donadini et al.*, 2007; *Stanton et al.*, 2011] with paleointensity sites that meet our site selection criteria and do not target transitional field states. Unfortunately these records are from the last few thousand years and do not provide comparable ages to the Antarctic dataset.

VADMs from this study and previously mentioned published data sets are plotted in Figure 7. For reference, we plot the paleomagnetic axial dipole moment model (PADM2M) of *Ziegler et al.* [2011]. All of the Antarctic intensity data (open diamonds) are lower than PADM2M and any contemporaneous high northerly latitude sites. Hemispheric asymmetry in average VADMs could explain a previously noted discrepancy between compilations of paleointensity from the global submarine basaltic glass data set and those from lava flows (e.g., *Tauxe and Yamazaki* [2007]), which until recently have been heavily biased toward northern hemisphere sampling sites. Moreover, it suggests that north-south asymmetry visible in the current geomagnetic field may persist for millions of years, as hinted at by previous studies (e.g., *Kelly and Gubbins* [1997]) and some numerical models with non-uniform boundary conditions (e.g., *Glatzmaier et al.* [1999]). Although evidence

from the Arctic and Antarctic suggest that hemispheric asymmetry exists, there simply are too few Arctic paleointensity records with sufficient temporal coverage to adequately evaluate this hypothesis.

Our directional data, however, allow us to examine high latitude northern hemisphere VGP dispersion, as quantified by S_F, and compare it to dispersion from high southerly latitudes. JM/SP has considerably fewer directional sites (N =37) than Antarctica (N =131), so in order to provide a more robust comparison we augment our Arctic directions by drawing all high latitude ($> 60^\circ$ N) directional studies from the MagIC database that meet our site selection criteria: $k_w \geq 50$, $nn \geq 5$, and a demagnetization code (DC) ≥ 4 or 5 (complete demagnetization of all specimens and the use of PCA to determine characteristic directions, *McElhinny and McFadden* [2000]). Some paleomagnetic studies have focussed their efforts on transitional sites and we exclude such studies in the present investigation. One study from Iceland meets all requirements [*Udagawa et al.*, 1999].

Jan Mayen/Spitsbergen, Antarctica and Iceland have different temporal distributions which may affect our comparisons of PSV. Antarctic paleodirections are predominantly 0-5 Ma (n=123/131) with eight sites scattered between 5-13 Ma. The bulk of the combined Arctic data (n=63/76) are 0-2 Ma with twelve sites between 2 and 9 Ma. We therefore limit our hemispheric comparison of PSV to the last 2 Ma. See Table 4 and Figure 8.

We correct for (the very small) plate motion by adjusting the sampling latitudes of all sites using the no-net-rotation plate motion model (NNR-MORVEL) of *Argus et al.* [2011]. In Figure 8, we compare high latitude VGP scatter from JM/SP, Iceland [*Udagawa et al.*, 1999] and Antarctica [*Lawrence et al.*, 2009]. We show S_F with all VGPs (Figure 8a), as well as dispersion calculated using the variable cutoff algorithm of *Vandamme* [1994] (Figure 8b). Open symbols are calculated for 0-2 Ma, closed symbols are 0-0.5 Ma. Predicted VGP dispersion from the PSV model TK03 [*Tauxe and Kent*, 2004] is plotted with no VGP latitudinal filter, 8a, and using the Vandamme cutoff, 8b. The dashed line in Figure 8b is the prediction from Model G [*McElhinny and McFadden*, 1997]. Note that Model G was designed to fit the PSVRL database [*McElhinny and McFadden*, 1997] which excludes VGPs according to the Vandamme variable cutoff method.

Unfiltered VGP dispersion for 0-2 Ma (open symbols) from Iceland and JM/SP are consistent with the prediction of the TK03 PSV model, although at the extreme end of the confidence bounds for JM/SP, while dispersion from Antarctica is at least 4° above TK03. When the Vandamme cutoff is used, Antarctic dispersion drops significantly and all locations have essentially the same value. This artificial suppression of VGP dispersion, coupled with our observation that the transformation from directions to VGPs makes the magnetic field appear more variable than the directions suggest, reinforces the argument that latitudinal VGP cutoffs should not be used for PSV analysis.

Our initial analysis of the last 2 Ma spans the Brunhes and Matuyama polarity chrons. S_F estimates derived from VGPs spanning reversals may differ from dispersion calculated during a single polarity interval. Paleodirections in the Matuyama chron have been shown to have a greater angular standard deviation about GAD than the Brunhes (e.g., *Johnson et al.* [2008]), in addition some sites may sample reversals, producing transitional directions that will cause an increase in S_F. To this end we analyze PSV from the last 0.5 Ma (closed symbols in Figure 8a) which, in theory, should produce more stable estimates of S_F. Mean VGP scatter in the Arctic decreases slightly to$25.1^{29.2}_{20.5}{}^\circ$ (n=26), while mean S_F in Antarctica increases to $33.4^{41.3}_{25.6}{}^\circ$ (n=29). Our interpretation of unfiltered dispersion for 0-0.5 Ma remains essentially the same as for 0-2 Ma, except the new Arctic estimate is in better agreement with TK03.

We observe that unfiltered VGP dispersion for 0-2 Ma in the Arctic is in good agreement with existing PSV models while scatter in Antarctica is significantly higher. This result, coupled with systematically low VADMs in Antarctica, hints at asymmetrical PSV behavior between the two high latitude regions for at least the last 0.5 Ma.

8. Conclusion

The comparison of high latitude directional and intensity data from both hemispheres suggests a significant zonal hemispheric asymmetry in the geomagnetic field that persists on timescales of 10^5-10^6 years. This asymmetry is not accounted for in existing secular variation models and requires long term non-axial-dipole field contributions. A significant quadrupolar component, 20% of the dipole field, would be needed to fit the asymmetry in field strength at high latitudes (although Arctic paleointensity records are sparse (n=5) and not yet conclusive). This high value is incompatible with observed inclination errors over the last 5 Ma (e.g., *Johnson et al.* [2008]) indicating that the long term geomagnetic field may contain some non-axial-dipole component or higher order terms as well.

The statistical parameters and percent of non-axial-dipole contribution in TK03 can easily be modified to fit our observed differences in polar VGP scatter, however, TK03 is a global model and changing parameters to fit asymmetries at high latitudes will have significant effects on PSV predictions at mid and low latitudes. Proper evaluation of the long term hemispheric asymmetry hypothesis requires globally distributed directional and intensity data spanning 10^5-10^6 years.

Existing numerical geodynamo simulations often explore geographic variations in thermal core-mantle boundary (CMB) conditions, especially potential cold regions around the Pacific rim, that could reflect seismic velocity variations near the CMB. Simulations with timescales of 100 kyrs or greater are often tested against TAF and PSV models with similar temporal resolution. The recent addition of high-quality paleomagnetic data, especially at equatorial (e.g., *Kent et al.* [2010]; *Opdyke et al.* [2010]) and high latitudes (e.g., *Lawrence et al.* [2009], *This Study*) allows for a greater understanding of long term geomagnetic field behavior and perhaps revisions to existing TAF and PSV models. If numerical geodynamo models can be made to reproduce the statistical behavior of these revised models, then it may be possible to understand the hemispherical asymmetries or other features seen in long term geomagnetic field behavior.

Acknowledgments. We thank Winfried Dallmann for significant logistical and field support in Spitsbergen and Leif-Erik Pedersen and Philip Staudigel for their hard work in the field collecting samples on Jan Mayen. We thank Brad Singer for his help with the ^{40}Ar/^{39}Ar experiments and for the use of his lab, and Bob Duncan for access to unpublished preliminary data from Jan Mayen. We appreciate Jason Steindorf's contributions to sample preparation and processing. Thanks to Jeff Gee for his constructive comments, and two anonymous reviewers who helped to greatly improve the manuscript. We are grateful to the crew of Jan Mayen, especially Ole Øiseth and Filip Myrvoll, for their hospitality and expertise. We thank Frank Vernon and Mert Ingraham for their assistance in adapting the Beeline differential GPS system for paleomagnetic work in Spitsbergen and Stephen Peter for training and troubleshooting with the ProMark3 GPS system. This material is based on work supported by National Science Foundation grants EAR9805164, EAR0838257, EAR0809709 and EAR1141840.

References

Argus, D. F., R. G. Gordon, and C. DeMets, Geologically current motion of 56 plates relative to the no-net-rotation reference frame, *Geochem. Geophys. Geosyst.*, *12*, 13, 2011.

Bloxham, J., The effect of thermal core-mantle interactions on the palaeomagnetic secular variation, *Phil Trans Roy Soc London, Series A*, *358*, 1171–1179, 2000.

Burov, Y., and I. Zagruzina, Results of a determination of the absolute age of Cenozoic basic rocks of the northern part of the island of Spitsbergen, *Geologija Sval'barda*, pp. 139–140, 1976.

Constable, C., and C. L. Johnson, Anisotropic paleosecular variation models: implications for geomagnetic field observables, *Physics of the Earth and Planetary Interiors*, *115*, 35–51, 1999.

Constable, C., and R. L. Parker, Statistics of the geomagnetic secular variation for the past 5 m.y., *J. Geophys. Res.*, *93*, 11,569–11,581, 1988.

Cox, A., Research note: Confidence limits for the precision parameter, K, *Geophys. J. Roy. Astron. Soc*, *17*, 545–549, 1969.

Dewey, J., and R. Strachan, Changing Silurian-Devonian relative plate motion in the Caledonides: sinistral transpression to sinistral transtension, *Journal of the Geological Society*, *160*, 219–229, 2003.

Donadini, F., M. Kovacheva, M. Kostadinova, L. Casas, and L. Pesonen, New archaeointensity results from Scandinavia and Bulgaria: Rock-magnetic studies inderence and geophysical application, *Phys. Earth Planet. Int.*, *165*, 229–247, 2007.

Dunlop, D., and O. Özdemir, Beyond Néel's theories: thermal demagnetization of narrow-band partial thermoremanent magnetization, *Phys. Earth Planet. Int.*, *126*, 43–57, 2001.

Fisher, R. A., Dispersion on a sphere, *Proc. Roy. Soc. London, Ser. A*, *217*, 295–305, 1953.

Fitch, F., A. Nairn, and C. Talbot, Palaeomagnetic studies on rocks from North Jan Mayen, *Norsk Polarinstitutt*, pp. 49–60, 1963.

Fitch, F., R. Grasty, and J. Miller, Potassium-argon ages of rocks from Jan Mayen and an outline of its volcanic history, *Nature*, *207*, 1965.

Glatzmaier, A., R. S. Coe, L. Hongre, and P. Roberts, The role of the Earth's mantle in controlling the frequency of geomagnetic reversals, *Nature*, *401*, 885–890, 1999.

Halvorsen, E., A paleomagnetic study of two volcanic formations from northern Spitsbergen., *Norsk Polarinstitutt*, pp. 70–75, 1972.

Harland, W., The geology of Svalbard, *Geological Society of London Memoir*, *17*, 1997.

Imsland, P., The geology of the volcanic island Jan Mayen Arctic Ocean, *Nordic Volcanological Institute*, 1978.

Imsland, P., The petrology of the volcanic island Jan Mayen Arctic Ocean, *Nordic Volcanological Institute*, 1980.

Johnson, C. L., et al., Recent Investigations of the 0-5 Ma geomagnetic field recorded in lava flows, *Geochemistry, Geophysics, Geosystems*, *9*, Q04,032, doi:10.1029/2007GC001,696, 2008.

Kelly, P., and D. Gubbins, The geomagnetic field over the past 5 million years, *Geophys. J. Int.*, *128*, 315–330, 1997.

Kent, D. V., H. Wang, and P. Rochette, Equatorial paleosecular variation of the geomagnetic field from 0-3 Ma lavas from the Galapagos Islands, *Physics of the Earth and Planetary Interiors*, *183*, 404–412, 2010.

Kirschvink, J. L., The least-squares line and plane and the analysis of paleomagnetic data, *Geophys. Jour. Roy. Astron. Soc.*, *62*, 699–718, 1980.

Korte, M., and C. Constable, The geomagnetic dipole moment over the last 7000 years–new results from a global model, *Earth and Planetary Science Letters*, *236*, 348–358, 2005.

Korte, M., C. Constable, F. Donadini, and R. Holme, Reconstructing the Holocene geoomagnetic field, *Earth and Planetary Science Letters*, *312*, 497–505, 2011.

Lawrence, K. P., C. G. Constable, and C. L. Johnson, Paleosecular variation and the average geomagnetic field at +/- 20 degrees latitude, *Geochemistry Geophysics Geosystems*, *7*, doi:10.1029/2005GC001,181, 2006.

Lawrence, K. P., L. Tauxe, H. Staudigel, C. Constable, A. Koppers, W. C. McIntosh, and C. L. Johnson, Paleomagnetic field properties near the southern hemisphere tangent cylinder, *Geochem. Geophys. Geosyst.*, *10*, *Q01005*, doi:10.1029/2008GC00,207, 2009.

Linder, J., and S. Gilder, Latitude dependency of the geomagnetic secular variation S parameter: A mathematical artifact, *Geophysical Research Letters*, *39*, 2012.

Lyberis, N., and G. Manby, Continental collision and lateral escape deformation in the lower and upper crust: An example from Caledonide Svalbard, *Tectonics*, *18*, 40–63, 1999.

Maher, H., A. Braathen, S. Bergh, W. Dallman, and W. Harland, Tertiary or Cretaceous age for Spitsbergen's fold-thrust belt on the Barents Shelf, *Tectonics*, *14*, 1321–1326, 1995.

McElhinny, M. W., and P. L. McFadden, Palaeosecular variation over the past 5 Myr based on a new generalized database, *Geophys. J. Int.*, *131*, 240–252, 1997.

McElhinny, M. W., and P. L. McFadden, Paleomagnetism: Continents and Oceans, *San Diego: Academic Press*, 2000.

McFadden, P. L., and M. W. McElhinny, The combined analysis of remagnetization circles and direct observations in paleomagnetism, *Earth Planet. Sci. Lett.*, *87*, 161–172, 1988.

Nagata, T., Y. Arai, and K. Momose, Secular variation of the geomagnetic total force during the last 5000 years, *J. Geophys. Res*, *68*, 5277–5282, 1963.

Opdyke, N., and K. Henry, A test of the dipole hypothesis, *Earth and Planetary Science Letters*, *6*, 139–151, 1969.

Opdyke, N., D. V. Kent, K. Huang, D. Foster, and J. Patel, Equatorial paleomagnetic time-averaged field results from 0-5 Ma lavas from Kenya and the latitudinal variation of angular dispersion, *Geochem. Geophys. Geosyst.*, *11*, 2010.

Pesonen, L., M. Leino, and H. Nevanlinna, Archaeomagnetic intensity in finland during the last 6400 years: Evidence for a Latitude-Dependent Nondipole Field at ∼AD 500, *J. Geomag. Geoelect.*, *47*, 19–40, 1995.

Prestvik, T., Cenozoic plateau lavas of Spitsbergen- a geochemical study, *Norsk Polarinstitutt*, pp. 129–143, 1977.

Shaar, R., H. Ron, L. Tauxe, R. Kessel, and A. Agnon, Paleomagnetic intensity derived from non-SD: Testing the Thellier IZZI technique on MD slag and a new bootstrap procedure, *Earth and Planetary Science Letters*, 2011.

Skjelkvale, B.-L., H. Amundsen, S. O'Reilly, W. Griffin, and T. Gjelsvik, A primitive alkali basaltic stratovolcano and associated eruptive centres, northwestern Spitsbergen: volcanology and tectonic significance, *Journal of Volcanology and Geothermal Research*, *37*, 1–19, 1988.

Stanton, T., P. Riisager, M. Knudsen, and T. Thordarson, New palaeointensity data from Holocene Icelandic lavas, *Physics of the Earth and Planetary Interiors*, *186*, 1–10, 2011.

Talwani, M., and O. Eldholm, Evolution of the Norwegian-Greenland Sea, *Geol. Soc. Amer. Bull.*, *88*, 969–999, 1977.

Tanaka, H., M. Kono, and H. Uchimura, Some global features of palaeointensity in geological time, *Geophys. J. Int.*, *120*, 97–102, 1995.

Tauxe, L., Essentials of Paleomagnetism, *University of California Press*, p. 489, 2010.

Tauxe, L., and D. V. Kent, A simplified statistical model for the geomagnetic field and the detection of shallow bias in paleomagnetic inclinations: Was the ancient magnetic field dipolar?, in *Timescales of the Paleomagnetic Field*, edited by e. a. Channell, J.E.T., vol. 145, pp. 101–116, American Geophysical Union, Washington, D.C., 2004.

Tauxe, L., and H. Staudigel, Strength of the geomagnetic field in the Cretaceous Normal Superchron: New data from submarine basaltic glass of the Troodos Ophiolite, *Geochem. Geophys. Geosyst.*, *5*, Q02H06, doi:10.1029/2003GC000,635, 2004.

Tauxe, L., and T. Yamazaki, Paleointensities, in *Geomagnetism*, edited by M. Kono, vol. 5 of *Treatise on Geophysics*, pp. 509–563, doi:10.1016/B978–044452,748–6/00,098–5, Elsevier, 2007.

Torsvik, T., R. Van der Voo, J. Meert, J. Mosar, and H. Walderhaug, Reconstructions of the continents around the North Atlantic at about the 60th parallel, *Earth and Planetary Science Letters*, *187*, 55–69, 2001.

Udagawa, S., H. Kitagawa, A. Gudmundsson, O. Hiroi, T. Koyaguchi, H. Tanaka, L. Kristjansson, and M. Kono, Age and magnetism of lavas in Jökuldalur area, Eastern Iceland: Gilsá event revisited, *Phys. Earth Planet. Int.*, *115*, 147–171, 1999.

Vagnes, E., and H. Amundsen, Late Cenozoic uplift and volcanism on Spitsbergen- Caused by mantle convection, *Geology*, *21*, 251–254, 1993.

Vandamme, D., A new method to determine paleosecular variation, *Phys. Earth Planet. Int.*, *85*, 131–142, 1994.

Wilson, R., Dipole Offset - Time-average palaeomagnetic field over past 25 million years, *Geophys. J. Roy. Astron. Soc*, *22*, 491–504, 1971.

Ziegler, L., C. Constable, C. L. Johnson, and L. Tauxe, PADM2M: a penalized maximum likelihood model of the 0-2 Ma palaeomagnetic axial dipole moment, *Geophys. J. Int.*, 2011.

Zijderveld, J., A.C. demagnetization of rocks: analysis of results, *Methods in Paleomagnetism*, pp. 254–286, 1967.

C.G. Constable, Institute of Geophysics and Planetary Physics, Scripps Institution of Oceanography, University of California San Diego, 9500 Gilman Dr, La Jolla, CA 92093-0225, USA

G. Cromwell, Geosciences Research Division, Scripps Institution of Oceanography, University of California San Diego, 9500 Gilman Dr, La Jolla, CA 92093-0220, USA

A.A.P. Koppers, College of Earth, Ocean and Atmospheric Sciences, Oregon State University, 104 CEOAS Admin Bldg, Corvallis, OR 97331-5503, USA

R-B. Pedersen, Department of Earth Science, Centre for Geobiology, University of Bergen, Postboks 7803, Bergen, Norway

H. Staudigel, Institute of Geophysics and Planetary Physics, Scripps Institution of Oceanography, University of California San Diego, 9500 Gilman Dr, La Jolla, CA 92093-0225, USA

L. Tauxe, Geosciences Research Division, Scripps Institution of Oceanography, University of California San Diego, 9500 Gilman Dr, La Jolla, CA 92093-0220, USA

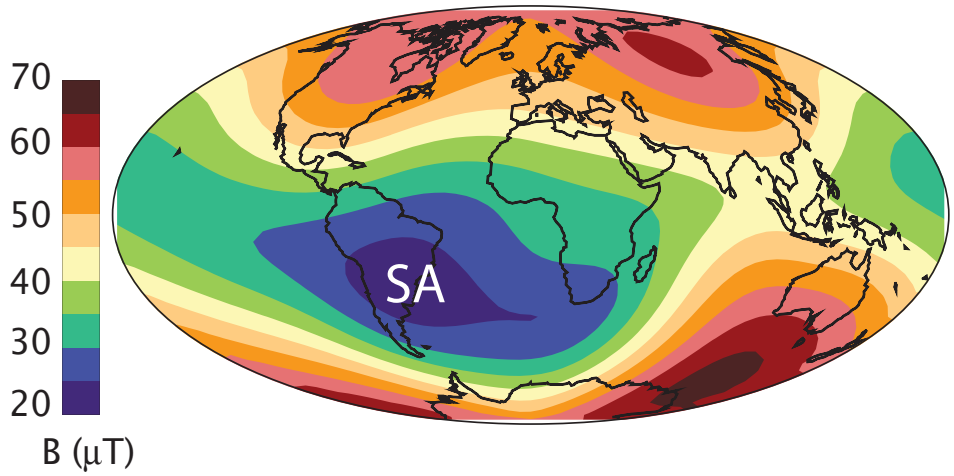

Figure 1. Present day geomagnetic field strength at the Earth's surface from the 2005 IGRF. SA indicates the general location of the South Atlantic Anomaly.

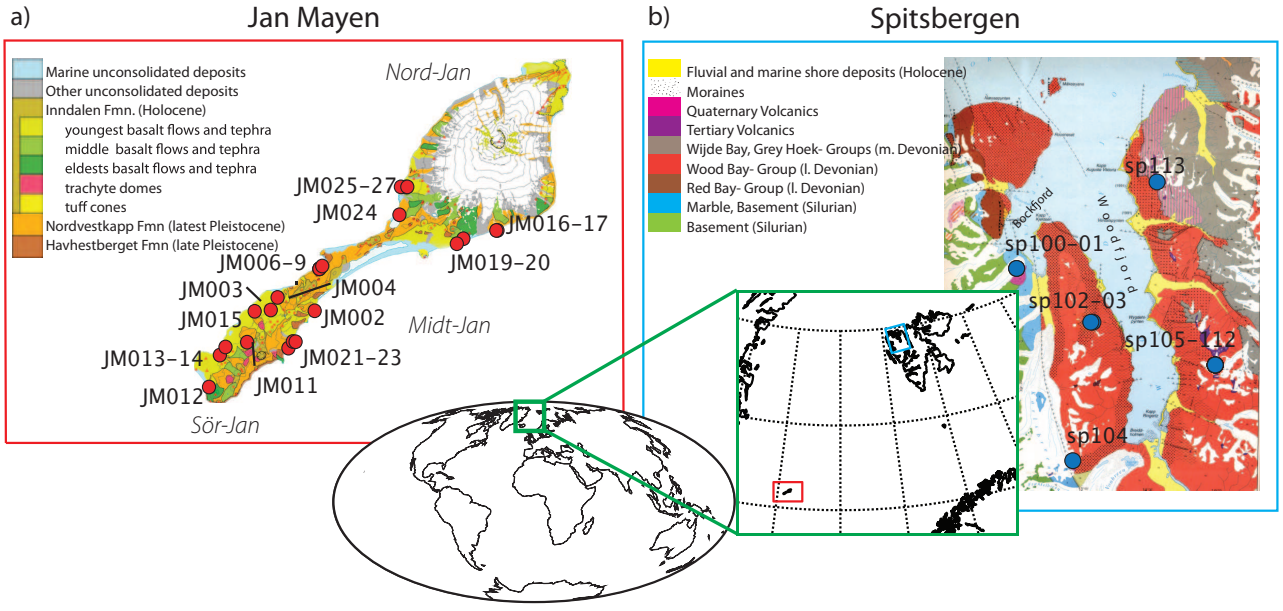

Figure 2. Locations of sampling sites from Jan Mayen and Spitsbergen. a) Map modified from the Geological map of Jan Mayen from the Norsk Polarinstitutt. Scale 1:250,000. Contour Interval 200 m. b) Map modified from the Geological Map of Woodfjorden Area (Haakon VII Land, Andreé Land), NW-Spitsbergen, Svalbard by M. Hoffman, G. Hell and K. Piepjohn, 1992. Scale 1:150,000.

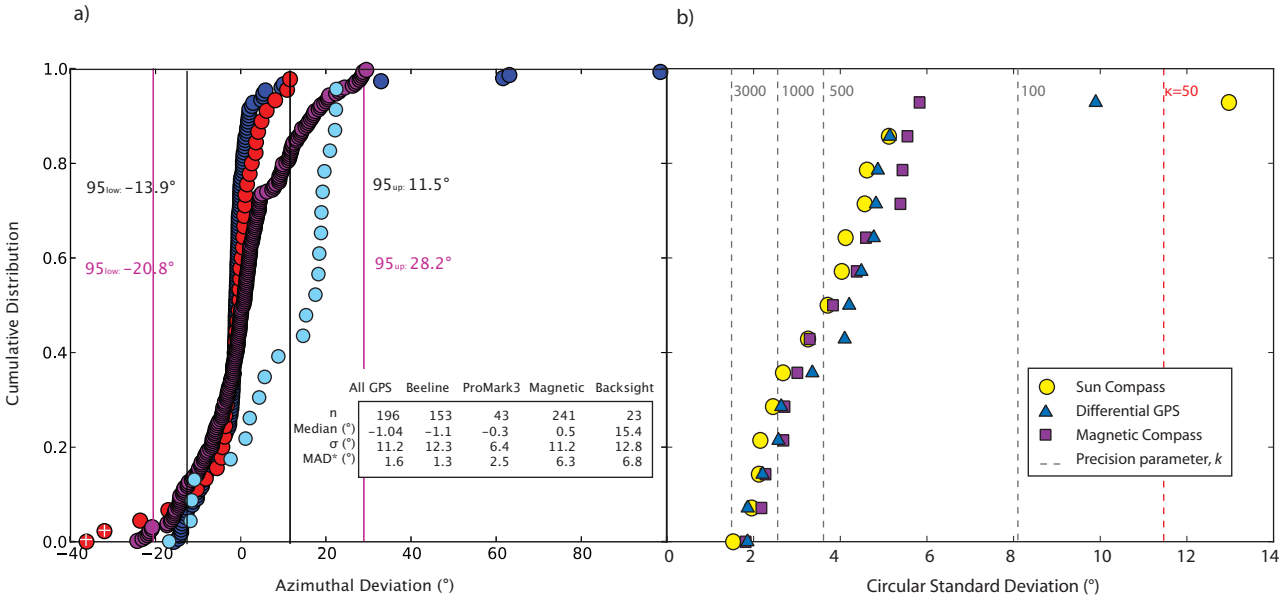

Figure 3. a) Cumulative distributions of deviations between sun compass azimuths and GPS Beeline (dark blue), ProMark3 GPS (red), magnetic compass (purple) and backsighted (light blue) azimuths. 95% confidence bounds of deviations for combined GPS (black) and magnetic (purple) measurements. White crosses indicate ProMark 3 GPS azimuths rejected due to insufficient satellite coverage. Inset table presents statistics of azimuth deviations for all orientation methods: n, number of sample azimuths; median azimuthal deviation from sun compass measurements; σ, standard deviation of the mean; MAD*, median absolute deviation. b) Cumulative distributions of the site mean circular standard deviation (°) for 14 sites with mean directions from sun compass, GPS, and magnetic compass orientation data. Equivalent values of the k precision statistic are plotted as dashed lines. Red dashed line is our site selection minimum value of k.

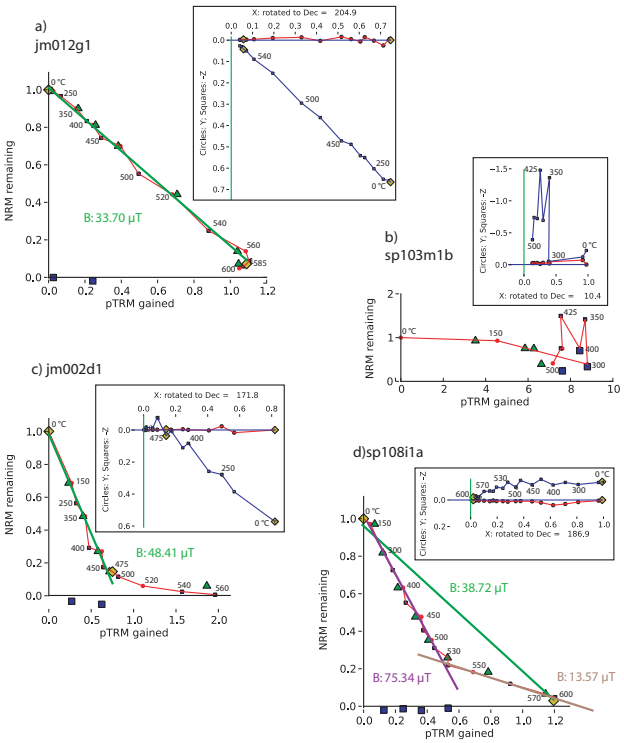

Figure 4. Arai plots of NRM remaining versus pTRM gained during IZZI-modified Thellier-Thellier paleointensity experiments for select specimens. Red circles (blue squares) represent ZI (IZ) heating steps. The green line is the estimated paleointensity component with the accompanying intensity value. pTRM checks are shown as small green triangles and pTRM tail checks are large blue squares. Insets are vector-endpoint (Zijderveld) diagrams where the x-axis has been rotated to the mean NRM direction. Circles (squares) are the horizontal (vertical) plane. Yellow diamonds represent the bounds used in the principal component analysis. a) jm012g1 (NRM normalized to 6.38 x 10^{-5} Am^2) are ideally behaved specimens. b) sp103m1b (5.94 x 10^{-5} Am^2) does not display ideal behavior. The specimen fails all pTRM checks and no intensity component can be derived. c) jm002d1 (8.07 x 10^{-5} Am^2) concave-up behavior occurs after a failed alteration check and is most likely a result of alteration. d) sp108i1a (8.22 x 10^{-5} Am^2) each line represents a different paleointensity estimation, all of which could be valid under certain selection criteria.

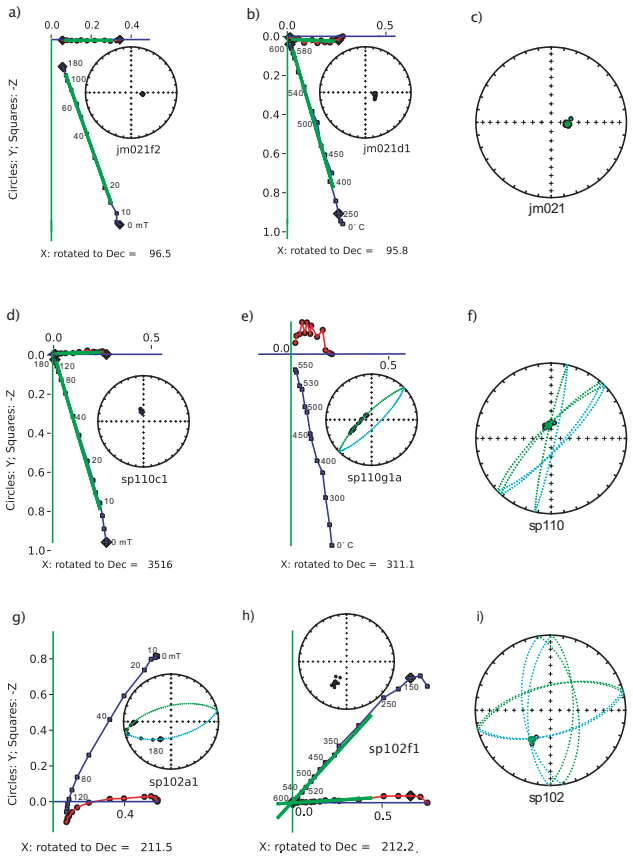

Figure 5. a-c) Typical "Type I" site. a) Thermal demagnetization shows straightforward, univectorial decay to the origin. Inset is plot of directions from each demagnetization step. b) AF demagnetization of sister specimen. Behavior is similar to thermal demagnetization. Inset same as (a). c) Directions of all best-fit lines defining characteristic directions similar to (a) and (b), site mean (green circle). d-f) "Type II" site. d) AF or thermal (not shown) demagnetization shows univectorial decay to the origin. Inset same as in (a). e) Demagnetization derived from Thellier (IZZI) experiment showing contamination from the applied lab field. Inset shows directions at each demagnetizaion step plotting as a great circle rather than a best-fit line. f) Same as (c) except includes great circle fits. g-h) Examples of GRM behavior.

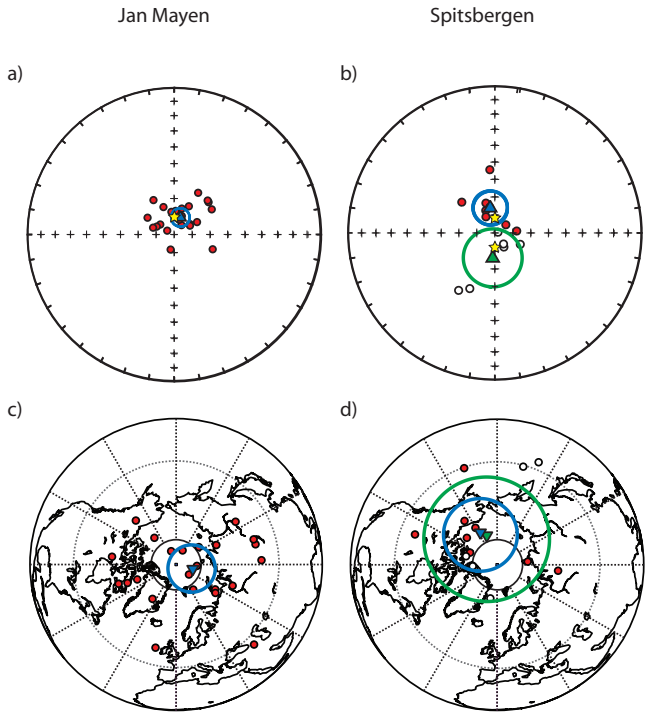

Figure 6. a, b) Equal area projections of site-mean directions. Filled (open) circles plot on the lower (upper) hemisphere. Grand mean directions (green triangles) with Fisher α_{95} confidence cones for normal (blue circle) and reversed (green circle) sites. Stars are expected directions from a GAD field. c, d) VGP positions for all sites. Dotted black circle is at 45° latitude, any sites below this line would be excluded in some studies applying VGP cutoffs. Filled (open) circles are northern hemisphere (antipodes of southern hemisphere) VGP positions. Blue (green) circles are Fisher α_{95} confidence cones for normal (reversed) VGPs.

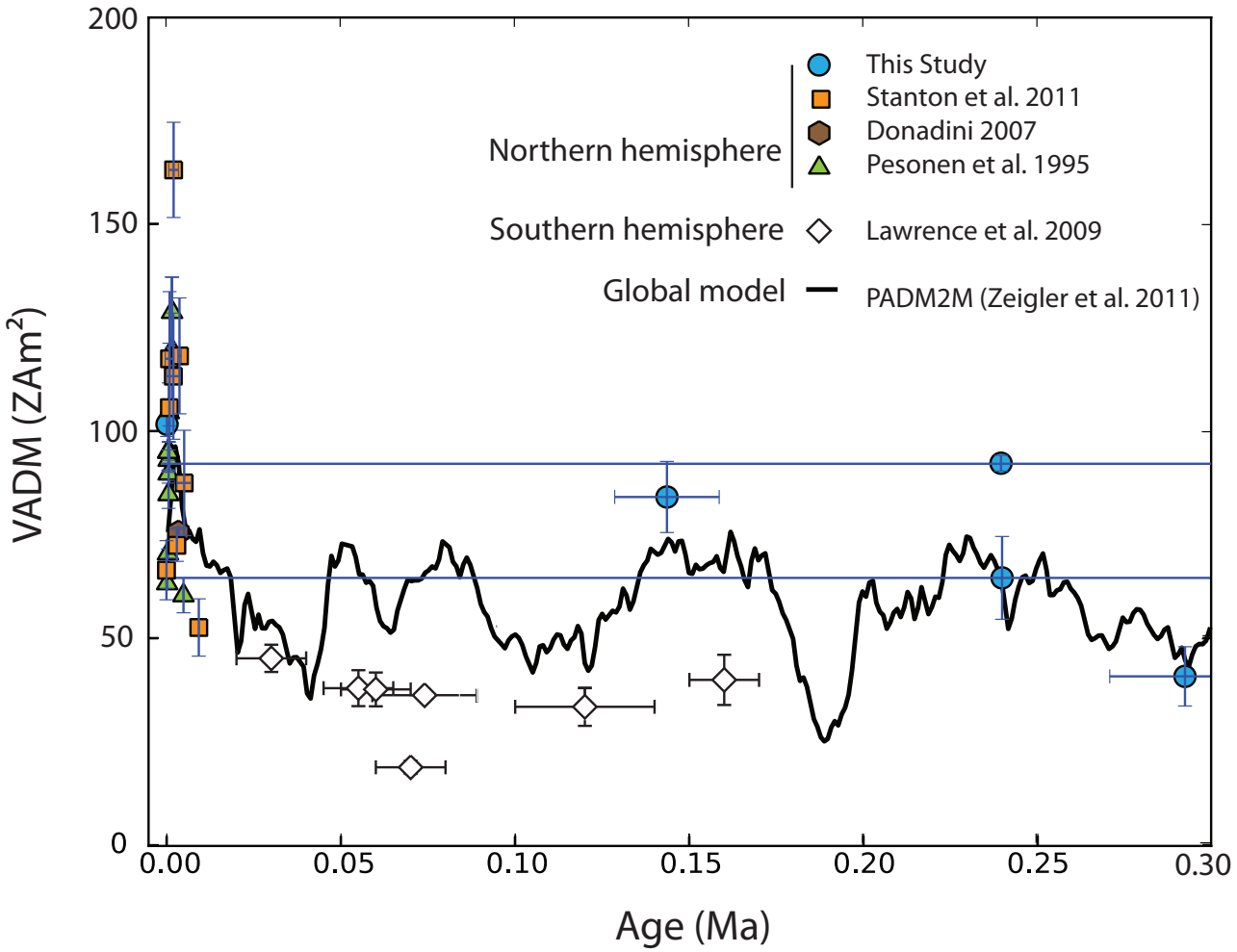

Figure 7. Virtual axial dipole moments (VADMs) for young, < 300 ka, sites at high northern latitude, $> 60^\circ$ N, and Antarctica. The PADM2M time-varying paleomagnetic axial dipole moment model is plotted for comparison. VADM errors are 2σ. Average VADM from Jan Mayen, $76.8 \pm 24.3(\sigma)$ ZAm^2, is a factor of two higher than Antarctica, $35.3 \pm 7.9(\sigma)$ ZAm^2. Sites used for VADM calculation, from youngest to oldest: Jan Mayen (n=5), JM020, JM021, JM002, JM019, JM012; Antarctica (n=8), mc218, mc13, mc225, mc200, mc09, mc35, mc36, mc217.

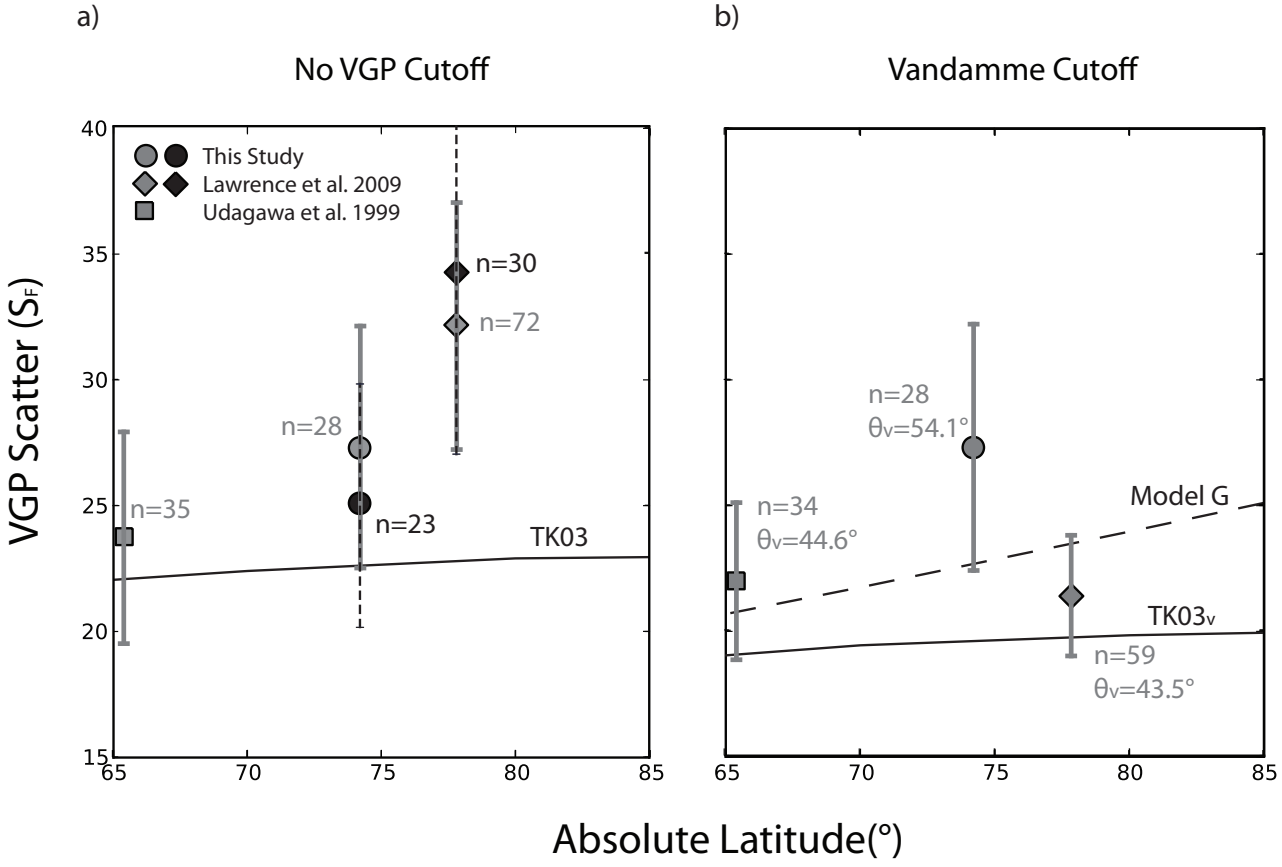

Figure 8. VGP scatter for 0-2 Ma (gray symbols) plotted against absolute latitude for Jan Mayen/Spitsbergen, Antarctica and Iceland with 95% confidence bounds. n is the number of sites for each location. 0-0.5 Ma dispersion (black symbols) plotted for JM/SP and Antarctica. a) VGP dispersion with no latitudinal cutoff. PSV model TK03. b) VGP dispersion using the variable Vandamme cutoff for 0-2 Ma (co-latitude cutoff value, θ_v, listed for each study). PSV models TK03$_v$ (solid) and Model G (dashed) [*McElhinny and McFadden*, 1997] are also plotted.

Table 1. Paleointensity results. N_B is the number of specimens used in paleointensity calculation. B (μT) is the average field strength at each site. σ_B is the standard deviation of the specimens used to calculate the site mean. $d\sigma_B$ is the standard deviation of the specimen intensities as a percent fraction of the mean intensity. VADM (ZAm^2) is the virtual axial dipole moment and σ_{VADM} is the standard deviation of specimens used to calculate the mean VADM. VDM is the virtual dipole moment, along with its standard deviation, σ_{VDM}

					B			VADM		VDM	
Site	Age (ka)	Lat (°N)	Lon (°E)	N_B	(μT)	σ_B	$d\sigma_B$	(ZAm^2)	σ_{VADM}	(ZAm^2)	σ_{VDM}
JM002	$<$ 460.9	70.9196	-8.71604	2	48.2	0.56	1.2	64.71	0.76	67.9	0.79
JM012	292.5$\pm$ 21.6	70.84644	-9.03706	4	30.36	3.64	12	40.94	4.91	48.8	5.85
JM019	$<$ 460.9	70.98853	-8.26443	2	68.56	6.74	9.8	92.4	9.08	112.4	11.05
JM020	1732 CE	70.98374	-8.28428	2	75.54	5.72	7.6	101.8	7.71	102.1	7.73
JM021	143.8$\pm$ 15.0	70.88377	-8.79582	3	62.48	2.91	4.7	84.24	3.92	91.3	4.25

Table 2. Jan Mayen site statistics. Age (ka) is calculated $^{40}Ar/^{39}Ar$ radiometric age with 2σ error or estimated age (see Geology and Sampling). All other flows are determined to be younger than the oldest surface flow, JM008. Dec and Inc are mean site declination and inclination, respectively. nl/np is the number of best-fit lines and planes, respectively, used in site mean calculations. N is the combined number of best-fit lines and planes. k is an estimate of the *Fisher* [1953] precision parameter, R is the resultant vector of N unit vectors, and $\alpha 95$ is the *Fisher* [1953] circle of 95% confidence. VGP Lat/Lon are the virtual geomagnetic poles calculated for each site. N_B is the number of specimens used in paleointensity calculation. Lat*, Lon*, PLat*, PLon* are site latitude, longitude and recalculated VGP lat and lon after adjusting for plate motion using the NNR-MORVEL model *Argus et al.* [2011].

Site	Age (ka)	Lat ($^\circ$N)	Lon ($^\circ$E)	Dec	Inc	nl/np/N	k_w	R	$\alpha 95$	VGP Lat	VGP Lon
JM002		70.9196	-8.71604	61.8	75.5	5/4/9	237	8.9747	3.5	65.6	69.4
JM003		70.92036	-8.84940	305.9	80.6	5/2/7	250	6.98	3.9	73.2	289.3
JM004	191.2$\pm$21.5	70.93240	-8.82873	3.9	76.9	5/2/7	304	6.9836	3.6	83.9	155.4
JM006	316.1$\pm$ 31.4	70.95979	-8.70165	302.3	72.6	5/1/6	409	5.989	3.4	63.3	262.3
JM007	329.3$\pm$ 16.2	70.95979	-8.70165	38.8	83.4	5/2/7	491	6.9898	2.4	78	34.3
JM008	460.9$\pm$ 55.8	70.95979	-8.70165	299	85.7	4/2/6	189	5.9789	5.1	73.4	324.2
JM009	429.6$\pm$ 19.1	70.96244	-8.69315	19.6	81.4	8/0/8	401	7.9825	4.6	83.6	52.1
JM011		70.88952	-8.92126	56.6	79.5	6/4/10	129	9.9456	5.5	71.6	57.6
JM012	292.5$\pm$ 21.6	70.84644	-9.03706	56.4	64.7	6/1/7	550	6.99	2.6	54.2	92.9
JM013		70.87710	-9.00407	22.9	78.9	8/0/8	154	7.9547	4.5	81.8	86.2
JM014		70.88490	-8.98695	47	63.6	5/1/6	54	5.9168	9.4	55.9	104.3
JM015		70.91912	-8.89832	294.5	79.5	6/0/6	86	5.9421	7.2	68.9	289.4
JM016	105.2$\pm$ 13.7	70.99645	-8.16072	111	66.9	5/1/6	308	5.9854	3.9	40.1	44.2
JM017		70.99642	-8.16439	353.4	77.4	7/0/7	241	6.9751	3.9	84.4	200.4
JM019		70.98853	-8.26443	44.8	63.3	6/4/10	484	9.9855	2.3	56.1	108.0
JM020	1732 CE	70.98374	-8.28428	61.2	79.9	5/1/6	146	5.9692	5.7	70.6	54.1
JM021	143.8$\pm$ 15.0	70.88377	-8.79582	27.8	72.3	8/0/8	619	7.9887	2.2	72.2	115.9
JM022	6.0$\pm$14.5	70.89018	-8.78241	30.1	63.1	4/3/07	531	6.9959	2.5	59.9	125.8
JM023		70.88992	-8.77403	329.1	67.7	5/0/5	67	4.9404	9.4	65.3	222.5
JM024		71.01136	-8.45861	287.9	77.8	4/3/7	113	6.9603	7.4	65.2	287.4
JM025		71.03788	-8.43919	16.8	75	5/2/7	1209	6.9959	1.8	78.7	127.5
JM026		71.03796	-8.45426	338.9	73.7	6/1/7	1096	6.995	2	75.8	219.3
JM027		71.03796	-8.43475	192.6	81.4	5/1/6	795	5.9943	2.4	54.4	345.3

Table 3. Spitsbergen site statistics. Age (Ma) is calculated $^{40}Ar/^{39}Ar$ radiometric age with 2σ error or estimated age (see Geology and Sampling). See Table 2 for a description of column definitions.

Site	Age (Ma)	Lat (°N)	Lon (°E)	Dec	Inc	nl/np/N	k_w	R	$\alpha 95$	VGP Lat	VGP Lon	Lat*	Lon*	PLat*	PLon*
SP100	< 1	79.44183	13.32802	53.5	82.4	5/2/7	1457	6.9966	1.6	77.9	96.1	79.31	12.78	77.9	95
SP101	< 1	79.44241	13.33350	85	77.8	6/3/9	915	8.9929	1.7	65.3	84.6	79.31	12.78	65.3	83.8
SP102	< 1	79.38689	13.71100	212.2	-51.7	3/4/7	403	6.9898	3.4	-41.1	337	79.26	13.15	-40.7	337.6
SP103	< 1	79.38746	13.70375	204.2	-55.7	5/2/7	537	6.9907	2.7	-45.8	345.4	79.26	13.14	-45.9	344.8
SP104	< 1	79.25779	13.60521	355.5	54.3	5/2/7	1413	6.9965	1.7	45.5	198.9	79.13	13.06	45.7	198.3
SP105	8.32±0.17	79.35397	14.31817	76.8	-88.2	6/3/9	385	8.9831	1.7	-78	177.2	78.28	9.96	-75.4	167.7
SP106	9	79.35379	14.31843	147.2	-80.7	11/1/12	291	11.964	2.5	-79.2	78.5	78.19	9.64	-77.8	76.5
SP107	9	79.35359	14.31884	141.7	-82.2	6/3/9	560	8.9884	2.2	-80.5	95.5	78.19	9.64	-80.6	97.7
SP108	9	79.35315	13.31942	338	76.6	7/2/9	369	8.981	2.7	73.9	229.9	78.19	9.64	74.9	227.7
SP109	9.15±0.16	79.35292	14.32005	343.4	72.7	6/3/9	87	8.9252	5.7	68.1	218.2	78.17	9.56	69.2	214.7
SP110	9	79.35190	14.32131	348.9	75.5	5/3/8	386	7.9857	2.9	73	211.9	78.19	9.64	74.1	208.5
SP111	9.09±0.14	79.35140	14.32131	313	64.8	6/3/9	1799	8.9964	1.2	53.3	251.4	78.19	9.64	53.9	248
SP112	9	79.35110	14.32136	114.1	-74.5	7/1/8	1625	7.996	1.4	-63.6	100.1	78.19	9.64	-63.7	97.7
SP113	9	79.52560	14.03114	331.2	79.8	5/3/8	608	7.9909	2.3	78.3	247.5	78.36	9.33	78.9	247.6

Table 4. VGP dispersion, S_F, with bootstrapped 95% confidence bounds, adjusted for plate motion using the NNR-MORVEL model of *Argus et al.* [2011]. S_F is calculated for Jan Mayen and Spitsbergen individually, combined sites from both locations, JM/SP, Iceland [*Udagawa et al.*, 1999], and Antarctica [*Lawrence et al.*, 2009]. Lat* is average location latitude corrected for plate motion [*Argus et al.*, 2011], N is number of sites used to calculate VGP scatter using no latitudinal cutoff, S_F, the iterative cutoff of *Vandamme* [1994], S_{Fv}, and a 45° cutoff, S_{F45}. λ_v is the Vandamme colatitudinal VGP cutoff .

Location	Lat*	N_F	$S_F(^\circ)$	N_{Fv}	$S_{Fv}(^\circ)$	λ_v	N_{F45}	$S_{F45}(^\circ)$
This Study								
Jan Mayen	70.9°	23	$24.4^{29.5}_{19.4}$	22	$22.5^{26.4}_{18.4}$	45.5°	22	$22.5^{26.4}_{18.4}$
Spitsbergen	78.6°	14	$28.4^{36.0}_{20.3}$	14	$28.4^{35.8}_{20.4}$	56.6°	13	$25.9^{32.9}_{18.0}$
All Sites								
Iceland	65.1°	38	$23.7^{27.5}_{19.9}$	37	$22.2^{25.1}_{19.3}$	45.4°	37	$22.2^{25.1}_{19.9}$
JM/SP	74.2°	37	$25.6^{29.6}_{21.2}$	37	$25.6^{30.0}_{21.1}$	51.3°	35	$23.4^{26.9}_{19.5}$
Antarctica	77.8°	131	$32.7^{36.8}_{28.9}$	120	$26.5^{28.9}_{24.1}$	52.6°	111	$23.6^{25.6}_{21.6}$
0-2 Ma								
Iceland	65.1°	35	$23.7^{29.7}_{19.7}$	34	$22.0^{25.1}_{18.9}$	44.6°	34	$22.0^{25.1}_{18.9}$
JM/SP	74.2°	28	$27.3^{32.1}_{22.3}$	28	$27.3^{32.2}_{22.5}$	54.1°	26	$24.7^{28.7}_{20.3}$
Antarctica	77.8°	72	$32.1^{37.0}_{27.1}$	59	$21.4^{23.8}_{19.0}$	43.5°	59	$21.4^{23.8}_{19.0}$
0-0.5 Ma								
JM/SP	74.2°	26	$25.1^{29.2}_{20.5}$	26	$25.1^{29.2}_{20.5}$	50.2°	25	$23.5^{27.5}_{19.1}$
Antarctica	77.8°	29	$33.4^{41.3}_{25.6}$	24	$22.8^{27.7}_{17.5}$	46.0°	23	$21.1^{25.5}_{16.3}$